UDC 544.47:546.26-162-31:[546.62-31+546.284-31]:547.261

V.V. Nosach [a, b], I.B. Bychko [a], P.Ye. Strizhak [a]

CATALYTIC PROPERTIES OF GRAPHENE OXIDE AND REDUCED GRAPHENE OXIDE SUPPORTED ON ALUMINA AND SILICA IN METHANOL CONVERSION

[a] L.V. Pisarzhevskii Institute of Physical Chemistry of National Academy of Sciences of Ukraine, Kyiv, Ukraine
[b] National University of «Kyiv-Mohyla Academy», Kyiv, Ukraine

The catalytic properties of graphene oxide and reduced graphene oxide supported on Al_2O_3 and SiO_2 were studied in methanol conversion. The results show the strong influence of the support and the chemical state of the graphene-derived phase on catalytic activity and product formation. SiO_2-supported catalysts provide low activity, whereas Al_2O_3-supported systems demonstrate significantly higher methanol conversion. Methanol conversion on Al_2O_3-supported materials leads to dimethyl ether formation in the intermediate temperature range, while at higher temperatures, methanol conversion shifts toward high-temperature products, including H_2, CO, CH_4, and CH_2O. This shift can be associated with diffusion limitations and surface coverage by the reduced graphene oxide phase. The study shows that methanol conversion pathways over graphene-derived catalysts can be tuned by combining oxide support properties with controlled reduction of graphene oxide.

Keywords*:* graphene oxide, reduced graphene oxide, alumina, silica, methanol conversion, carbocatalysis.

DOI: 10.32434/0321-4095-2026-164-1-157-168

Introduction

Catalytic conversion of methanol is a key area of contemporary chemical science and technology, as methanol is a widely available platform molecule, a potential energy carrier, and a versatile feedstock to produce value-added chemicals. Depending on the reaction conditions and the catalyst, methanol can follow different transformation pathways. Among the most significant methanol transformation pathways are dehydration to dimethyl ether (DME) and high-temperature reactions leading to the formation of gaseous products and oxygenated compounds, particularly formaldehyde (CH_2O) [1].

Dimethyl ether is regarded as a potential alternative to liquefied petroleum gas and methanol dehydration to DME, which provides a significant practical and scientific interest [1]. This reaction mainly proceeds on acidic catalytic sites, especially on γ-Al_2O_3 surfaces, where weak-to-moderate Lewis acid sites play a key role [2,3]. At the same time, DME selectivity and catalytic performance strongly depend on surface acid-base properties and competitive adsorption of water formed as a coproduct [1,4]. Another important research direction is direct high-temperature methanol conversion toward formaldehyde and hydrogen, which is considered a potentially attractive but challenging process in terms of selectivity control and catalyst stability [1]. Conventional industrial formaldehyde production relies on microcrystalline silver or mixed-oxide catalysts, mainly $Fe_2(MoO_4)_3$ [5]. However, in oxygen-containing atmospheres such systems promote undesired side

reactions, including CO/CO_2 formation and deep methanol degradation [1].

An alternative approach actively developing in recent years is the utilization of carbocatalysts, which involves using carbon materials as metal-free catalysts or functional modifiers of oxide supports. Carbon nanomaterials show acid–base and redox behavior due to structural defects and surface functional groups [6]. Graphene oxide has been widely reported as an efficient metal-free carbocatalyst and solid acid catalyst in various organic transformations, which is commonly attributed to oxygen-containing surface groups [6–8]. In addition, graphene oxide has been shown to catalyze reactions involving methanol as a substrate in the synthesis of oxygenated ethers [9]. In contrast, reduced graphene oxide contains fewer oxygen functionalities but a higher fraction of sp^2 carbon and distinct defect features, which may substantially alter its catalytic behavior [10]. In supported systems, the catalytic performance of graphene-derived phases is additionally influenced by the physicochemical properties of the oxide matrix.

Combining graphene derivatives with oxide supports such as SiO_2 and Al_2O_3 represents a promising strategy for designing catalysts with tunable surface and textural properties. These oxides differ significantly in their acid–base characteristics and interaction with alcohol molecules. SiO_2 is generally characterized by weak surface acidity and high chemical inertness, which limits its direct participation in methanol conversion and suggests that the catalytic activity of SiO_2-supported systems is mainly associated with the graphene-derived phase. In contrast, γ-Al_2O_3 provides a higher density of Lewis acid sites and surface hydroxyl groups, which are known to facilitate methanol dehydration reactions [2,3]. The overall catalytic behavior may result from the combined or overlapping contributions of the oxide support and the deposited graphene-derived phase, which can significantly affect both methanol activation and product distribution. However, the influence of graphene oxide reduction degree and the interaction between the carbon phase and oxide matrix on selectivity toward DME, CH_2O, H_2, CO, and CH_4 remains insufficiently understood and requires systematic investigation [1,6].

In the present work, supported on SiO_2 and Al_2O_3 graphene oxide- and reduced graphene oxide-based catalysts were studied in methanol conversion over a wide temperature range. The samples were prepared by depositing an aqueous graphene oxide suspension onto oxide supports, followed by reduction in a hydrogen atmosphere to obtain the rGO-containing materials. The catalysts were characterized by Raman spectroscopy, FTIR, SEM–EDS, thermogravimetric analysis, and low-temperature nitrogen adsorption–desorption measurements. This study focuses on comparing methanol conversion and the temperature-dependent formation of DME, CH_2O, H_2, CO, and CH_4 as a function of the support nature and the state of the graphene-derived phase.

Experimental

Samples containing graphene oxide (GO) and reduced graphene oxide (rGO) supported on silica and alumina were prepared by impregnation of the supports with an aqueous GO suspension. The GO suspension was obtained by exfoliation of graphite oxide (GrO), which was synthesized using a modified Hummers' method followed by ultrasonic treatment [11]. Aluminum oxide and silica powders with a particle size of 0.25–0.5 mm were impregnated at a ratio of 1 mL of suspension per 1 g of support. After impregnation, the samples were dried at 60^0C for 3 h. The GO-containing samples were used after this drying step, whereas the rGO-containing samples were obtained by an additional reduction step in a hydrogen flow at 400^0C for 2 h, which resulted in partial removal of oxygen-containing functional groups and formation of a reduced graphene oxide phase. A series of catalysts with a GO or rGO loading of 1 mg/g was prepared and denoted according to the support and graphene material as GO/SiO_2, rGO/SiO_2, GO/Al_2O_3, and rGO/Al_2O_3.

The structural properties and surface functionalities of the obtained samples were investigated using scanning electron microscopy (SEM) with an energy-dispersive spectroscopy analyser (EDS), Fourier transform infrared spectroscopy (FTIR), Raman spectroscopy, thermogravimetric analysis (TGA) and low-temperature nitrogen adsorption-desorption analysis. The morphology and spatial distribution of elements in the samples containing rGO and GO were examined by SEM using a Quanta 3D FEG microscope equipped with an EDS analyzer. FTIR spectra were recorded with a Perkin Elmer «Spectrum One» spectrometer in the range of 400–4000 cm^{-1}. Raman spectra were recorded at room temperature using a Raman Senterra confocal dispersive spectrometer (Bruker Optik) with 532 nm excitation and a laser power of 2 mW. Thermogravimetric analysis (TGA) was performed on a Thermoanalyzer Discovery SDT 650 instrument in air and nitrogen atmospheres at a heating rate of 10^0C min^{-1} to evaluate thermal stability and determine the carbon content of the samples. The textural characteristics of the samples were determined from nitrogen adsorption–desorption isotherms measured at 77 K using a Sorptomatic 1990

instrument by the volumetric method.

Methanol conversion was evaluated in a fixed-bed flow reactor at atmospheric pressure. The experiments were carried out in the temperature range of 100–550°C using a quartz tubular reactor with an inner diameter of 10 mm. In all experiments, 0.1 g of catalyst was placed in the reactor between two layers of quartz wool. The total feed flow rate was 70 sccm, consisting of 50 sccm Ar and 20 sccm CH_3OH, corresponding to a WHSV of 17.1 h^{-1}. Methanol was introduced by passing the argon stream through an evaporator. Blank tests performed in an empty reactor and in a reactor filled only with quartz wool showed no methanol conversion, confirming the absence of secondary reactions. Reaction products were analyzed using two gas chromatographs: a Chrom-5 instrument equipped with a flame ionization detector and a Hewlett Packard DB-2 capillary column, and an LHM-80 instrument equipped with a thermal conductivity detector and a Porapak-Q column.

The methanol conversion was calculated using the following relation:

$$X = \left(1 - \frac{C_{MeOH}}{C^0_{MeOH}}\right) \cdot 100\%,$$

where C^0_{MeOH} and C_{MeOH} are the initial methanol concentration and the concentration of the unreacted methanol in the reaction mixture, respectively.

The composition of the gas mixture after methanol conversion was calculated using the following relation:

$$C_i = \left(\frac{C_i}{\sum C_i}\right) \cdot 100\%,$$

where C_i is the concentration of product i; and ΣC_i is the total concentration of all detected products in the reaction mixture.

Results and discussion

Figure 1 presents SEM images of the pristine oxide supports SiO_2 and Al_2O_3 together with the corresponding GO- and rGO-modified samples. SEM–EDS analysis of pristine SiO_2 shows a surface composition dominated by oxygen and silicon, with oxygen in the range of 60–65 wt.% and silicon 30–35 wt.%, while the carbon contribution is minor, around 3 wt.%. Such a composition is typical for porous silica materials and the detected carbon can be attributed to surface-adsorbed carbon-containing species. Deposition of graphene oxide and reduced graphene oxide on SiO_2 leads to a pronounced increase in the detected carbon content to approximately 15 wt.%, accompanied by a strong attenuation of the silicon signal to below 2 wt.%, while oxygen remains the dominant element at with 80–85 wt.%. These changes indicate the formation of carbon-rich regions on the silica surface and suggest preferential localization of the graphene-derived phase on the outer surface of the support.

SEM–EDS analysis of the pristine Al_2O_3 support reveals a surface composition dominated by oxygen and aluminum, with oxygen in the range of 55–60 wt.% and aluminum 35–40 wt.%, whereas the carbon contribution remains low at 5–6 wt.%. Modification with graphene oxide and reduced graphene oxide results in a gradual increase in the carbon content to 8–9 wt.%, while the relative contributions of oxygen and aluminum remain nearly unchanged. The small difference in carbon content between GO/Al_2O_3 and rGO/Al_2O_3, which lies within the experimental uncertainty of EDS analysis, suggests that the reduction step primarily affects the chemical state of the graphene-derived layer rather than its overall surface coverage.

The FTIR spectrum of pristine SiO_2 is characterized by intense absorption bands in the 3700–3000 cm^{-1} region, associated with O–H stretching vibrations of surface silanol groups and adsorbed water, as well as a strong band near ~1100 cm^{-1} corresponding to asymmetric Si–O–Si stretching vibrations of the silica framework [12]. In addition, a distinct band observed in the ~800–750 cm^{-1} region can be assigned to symmetric Si–O–Si stretching and bending modes, which are typical for amorphous silica. The FTIR spectrum of pristine Al_2O_3 differs from that of SiO_2 and is dominated by broad absorption features related to surface hydroxyl groups and adsorbed water, together with wide Al–O lattice vibration bands mainly distributed in the 1000–800 cm^{-1} region and at lower wavenumbers, which are characteristic of γ-Al_2O_3 [13].

Deposition of graphene oxide and reduced graphene oxide on both oxides supports leads to the appearance of additional spectral features that are not present in the pristine materials. In particular, new contributions emerge in the 1250–1000 cm^{-1} region and near ~1600 cm^{-1} for both GO- and rGO-containing samples [14]. The bands in the 1250–1000 cm^{-1} range can be attributed to vibrations of oxygen-containing functional groups of graphene oxide (C–O and C–O–C), which overlap with the intense framework vibrations of the oxide supports but nevertheless indicate the presence of a carbonaceous phase on the surface. The absorption near ~1600 cm^{-1} is associated with skeletal vibrations of sp^2-hybridized carbon domains (C=C) and may also include contributions from the bending mode of

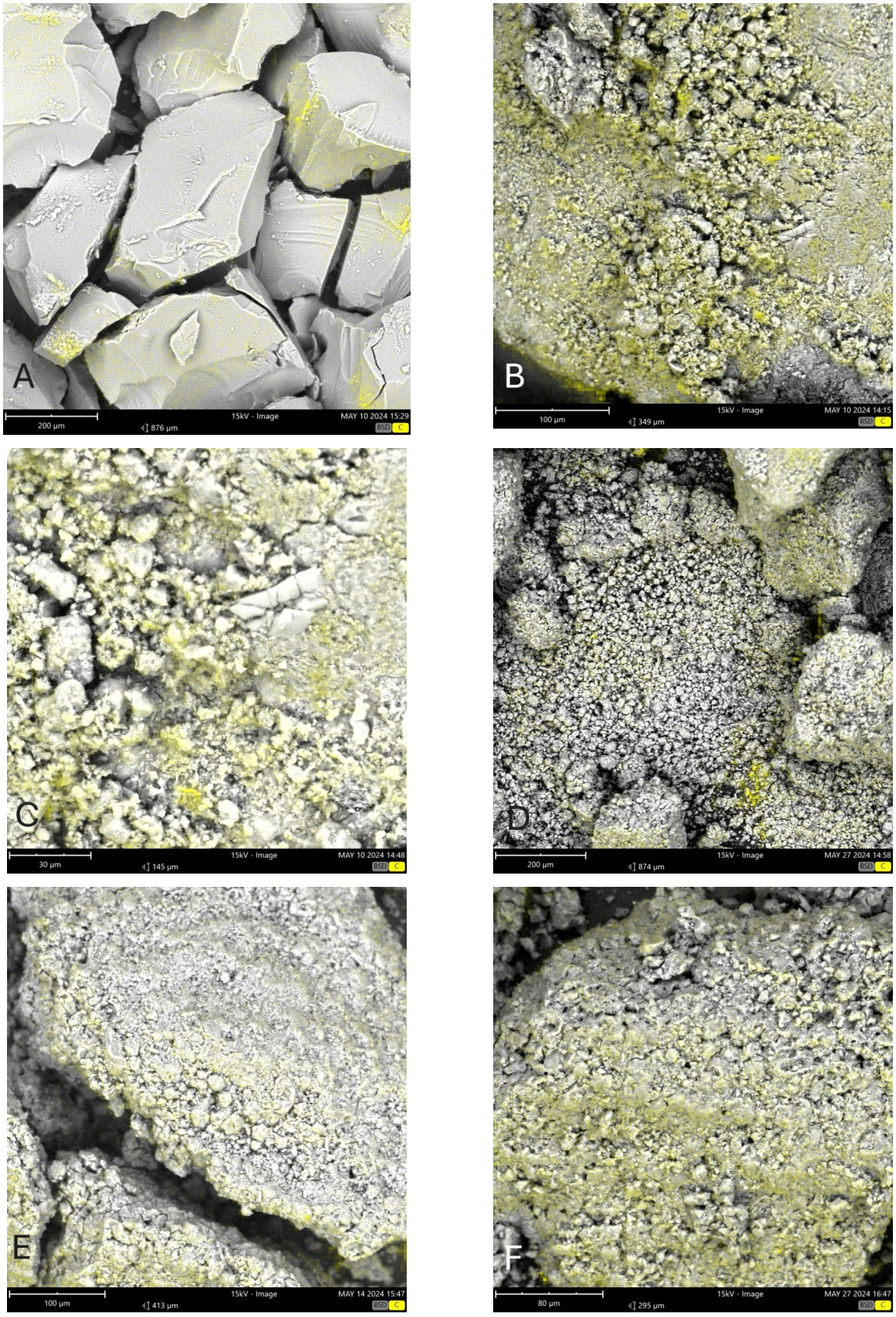

Fig. 1. SEM images of the samples: (a) SiO_2; (b) GO/SiO_2; (c) rGO/SiO_2; (d) Al_2O_3; (e) GO/Al_2O_3; (f) rGO/Al_2O_3

adsorbed water (δ H–O–H), which is commonly observed for porous oxide materials [15]. For the rGO-modified samples on both SiO_2 and Al_2O_3, a decrease in the intensity of the 1250–1000 cm^{-1} region is observed together with a relative enhancement of the ~1600 cm^{-1} band compared with the corresponding GO-containing samples. This behavior is consistent with partial removal of oxygen-containing functional groups during the reduction process and a higher contribution of restored sp^2 carbon structures in rGO [15].

Figure 2b shows the Raman spectra of SiO_2, Al_2O_3, GO/SiO_2, rGO/SiO_2, GO/Al_2O_3, and rGO/Al_2O_3 in the 1000–3000 cm^{-1} range. No intense Raman bands are detected for the pristine SiO_2 and Al_2O_3 supports, which is consistent with literature data for amorphous silica and γ-Al_2O_3 in this spectral region [16,17]. After deposition of graphene oxide, the spectra of GO/SiO_2 and GO/Al_2O_3 show characteristic D and G bands located at approximately 1350 and 1600 cm^{-1}, respectively, confirming the presence of graphene-based carbon structures on both oxide supports [17,18]. After reduction, the rGO/SiO_2 and rGO/Al_2O_3 samples show an increase in the intensities of the D and G bands, and a higher ID/IG ratio compared with the corresponding GO-based catalysts. This indicates an increased defect density and a higher degree of structural disorder in the carbon phase after the GO-to-rGO conversion, which is commonly reported for reduced graphene oxide due to partial removal of oxygen-containing groups accompanied by the formation of new defects in the spI carbon framework [19–21]. A distinct 2D band near 2700 cm^{-1} is not clearly observed for any of the supported samples, suggesting limited long-range graphitic ordering of the deposited carbon phase. Overall, the Raman results confirm successful formation of GO- and rGO-derived structures on both supports and demonstrate that reduction increases the defectiveness of the graphene-based phase.

The results of nitrogen adsorption–desorption isotherm analysis of the investigated samples are summarized in Table 1. Pristine SiO_2 shows the highest specific surface area, 375 $m^2 \cdot g^{-1}$, and a pronounced micropore volume, 0.12 $cm^3 \cdot g^{-1}$, at a total pore volume 0.85 $cm^3 \cdot g^{-1}$. Deposition of graphene oxide on SiO_2 leads to a decrease in the specific surface area to 320 $m^2 \cdot g^{-1}$ and an increase in the total pore volume to 0.95 $cm^3 \cdot g^{-1}$. At the same time, the micropore volume strongly decreases to 0.02 $cm^3 \cdot g^{-1}$, indicating a substantial reduction of microporosity after carbon deposition. A similar trend is observed for rGO/SiO_2, which also exhibits a surface area of 320 $m^2 \cdot g^{-1}$ and a total pore volume of 0.95 $cm^3 \cdot g^{-1}$. At the same time, the micropore volume decreases further to ≤0.01 $cm^3 \cdot g^{-1}$. Consequently, modification of silica with GO or rGO leads to partial blockage of micropores and a reduction in the accessible surface area, whereas the total pore volume remains relatively high.

The pristine Al_2O_3-based support exhibits a lower specific surface area of 245 $m^2 \cdot g^{-1}$ and a smaller total pore volume of 0.65 $cm^3 \cdot g^{-1}$, and the micropore volume is very low at ≤0.01 $cm^3 \cdot g^{-1}$ in comparison with SiO_2. Following graphene oxide deposition, the GO/Al_2O_3 sample shows only minor variations in textural properties, with a specific surface area of 240 $m^2 g^{-1}$ and a total pore volume of 0.60 $cm^3 \cdot g^{-1}$. The micropore volume remains unchanged at ≤0.01 $cm^3 \cdot g^{-1}$. The rGO/Al_2O_3 sample shows similar characteristics, with 240 $m^2 \cdot g^{-1}$, 0.65 $cm^3 \cdot g^{-1}$, and 0.01 $cm^3 \cdot g^{-1}$, indicating that reduction of the graphene oxide phase does not significantly affect the textural parameters of Al_2O_3-supported systems. Overall, carbon deposition exerts a more pronounced influence on the porous structure of SiO_2-supported samples, whereas

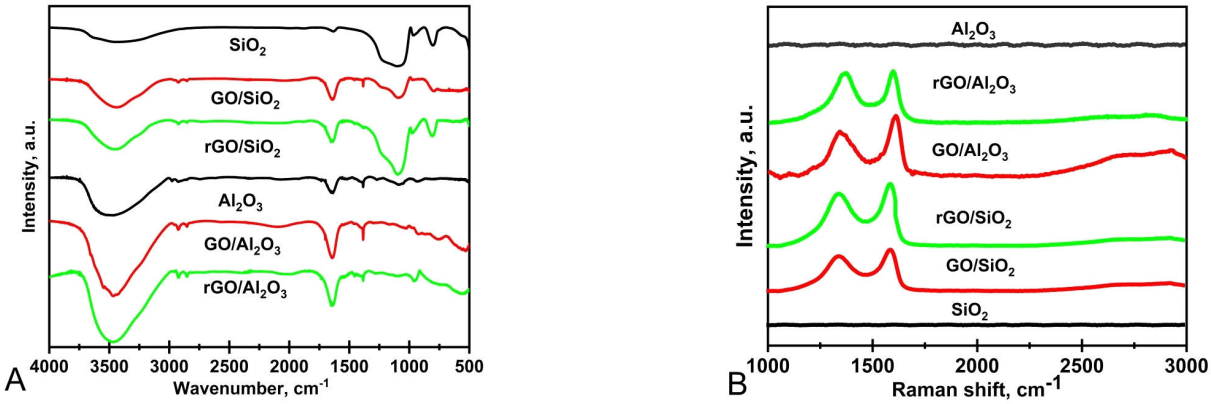

Fig. 2. FTIR (a) and Raman (b) spectra of SiO_2, Al_2O_3; GO/SiO_2; rGO/SiO_2; GO/Al_2O_3; and rGO/Al_2O_3

the textural characteristics of Al_2O_3-supported materials remain largely unaffected by GO or rGO deposition.

Thermogravimetric measurements of GO/Al_2O_3 and rGO/Al_2O_3 were performed under nitrogen and air atmospheres. In the 30–150°C temperature range, both materials undergo mass loss due to desorption of physically adsorbed water. This contribution amounts to ~6% for GO/Al_2O_3 and ~5–6% for rGO/Al_2O_3, reflecting the higher concentration of polar hydroxyl and epoxy groups in graphene oxide compared with reduced graphene oxide [22–24]. The 150–700°C temperature range corresponds to the main decomposition stage. In this range, GO/Al_2O_3 loses ~6% of its mass, which is attributed to extensive decomposition of oxygen-containing functional groups, including hydroxyl, epoxy, carbonyl, and carboxyl species [23–26]. In contrast, rGO/Al_2O_3 shows a smaller mass loss of ~5%, consistent with the lower content of residual oxygen functionalities after reduction [23–26]. In air, this process additionally involves oxidation-related transformations of the carbon phase, although the overall mass loss remains comparable to that observed in nitrogen [25,26]. Above 700°C, both samples undergo only minor additional mass loss of ~1%, indicating high thermal stability of the remaining carbonaceous residue [25,26]. Consequently, the total mass loss reaches ~12% for GO/Al_2O_3 and ~10–11% for rGO/Al_2O_3 over the 30–1000°C temperature range of the carbon phase. The higher total mass loss of GO/Al_2O_3 by approximately 1–2% relative to rGO/Al_2O_3 is primarily attributed to the greater amount and lower thermal stability of oxygen-containing functional groups in graphene oxide, which undergo extensive decomposition upon heating [22–25]. In contrast, the reduced graphene oxide-based sample contains fewer such labile functionalities and therefore undergoes a more limited overall mass loss [23–26].

Thermogravimetric measurements of the rGO/SiO_2 sample were performed under nitrogen and air atmospheres. In an inert atmosphere, the total mass loss over 30–1000°C is limited to ~5%, indicating a lower content of thermally labile surface species compared with the alumina-based composites [25,26]. The low-temperature region 30–150°C contributes only ~1% weight loss, reflecting weaker water retention by the silica-supported rGO and the presence of a relatively small amount of residual oxygen-containing groups after reduction [22,25]. The main mass loss of ~1.5–2% occurs between 150 and 700°C and is associated with the removal of remaining oxygen functionalities and partial degradation of defective carbon fragments [23–25]. Above 700°C, only a minor additional decrease of ~1–2% is observed, confirming the high thermal stability of the carbon phase [24,25]. In air, the overall weight loss slightly increases to ~6% [25,26]. While the decomposition pattern remains similar, the intermediate temperature range 150–700°C is additionally affected by oxidative transformations

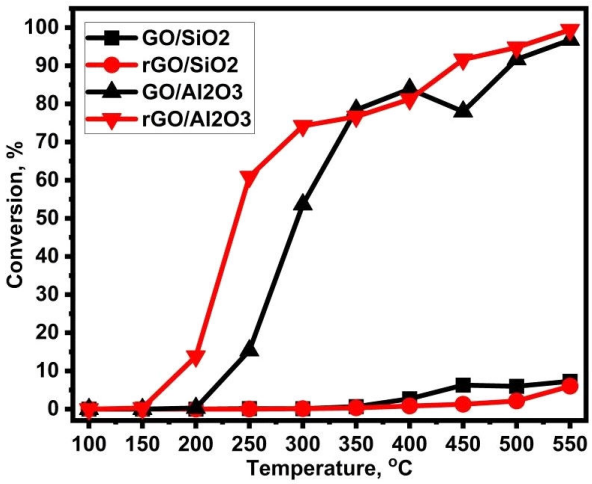

Fig. 3. Temperature dependence of methanol conversion in the temperature range of 100–400°C, total feed flow rate 70 sccm, consisting of 50 sccm Ar and 20 sccm CH_3OH, corresponding to a WHSV of 17.1 h^{-1}. Methanol conversion on GO/SiO_2 – ■; rGO/SiO_2 –●; GO/Al_2O_3 – ▲; rGO/Al_2O_3 – ▼

Table 1

Textural characteristics of SiO_2, Al_2O_3, GO/SiO_2, rGO/SiO_2, GO/Al_2O_3, and GO/Al_2O_3 samples

Sample	Specific surface area, S, $m^2 \cdot g^{-1}$	Total pore volume, V_p, $cm^3 \cdot g^{-1}$	Micropore volume, V_m, $cm^3 \cdot g^{-1}$
SiO_2	375	0.85	0.12
GO/SiO_2	320	0.95	0.02
rGO/SiO_2	320	0.95	≤0.01
Al_2O_3	245	0.65	≤0.01
GO/Al_2O_3	240	0.60	≤0.01
rGO/Al_2O_3	240	0.65	≤0.01

of the carbon component, leading to a mass loss of ~2–3% [23,25]. At higher temperatures 700–1000°C, the further ~2% decrease is attributed to the final oxidation of the rGO framework, which remains largely preserved under nitrogen [24–26].

Figure 3 shows the temperature dependence of methanol conversion over the GO/SiO_2, rGO/SiO_2, GO/Al_2O_3, and rGO/Al_2O_3 samples. For the SiO_2-based catalysts GO/SiO_2 and rGO/SiO_2, methanol conversion remains low across the entire temperature range, with a noticeable increase only above at 400°C, reaching 2.5%, indicating the low catalytic activity of these samples. In contrast, the Al_2O_3-based catalysts show significantly higher activity. For the rGO/Al_2O_3 sample, a sharp increase in conversion is observed at the range of 200–250°C, after which the conversion rises rapidly and reaches ~70–80% at 300–350°C. Further temperature increase, it continues to increase more gradually, approaching 97% at 550°C. Conversion for the GO/Al_2O_3 catalyst also starts to increase at in the range of 200–250°C but rises less steeply, reaching 80% at 400°C. In the higher-temperature region, the conversion rises 99% at 550°C. Overall, the Al_2O_3-supported samples are considerably more active than the SiO_2-supported ones, and among them, rGO/Al_2O_3 demonstrates the earliest onset of methanol conversion and the highest, most stable conversion over a wide temperature interval.

Figure 4a presents the temperature dependence of the product composition during methanol conversion over the GO/SiO_2 catalyst. In the 350–450°C temperature range, methanol conversion increases markedly, accompanied by the formation of products other than MeOH. In this range, DME and H_2O are the dominant products within the converted fraction, indicating activation of the methanol dehydration pathway. The DME contribution reaches its maximum in the 350–450°C range and then gradually decreases with further heating. In the temperature region 450–550°C, the amount of gaseous products increases, particularly H_2 and CO, along with the formation of CH_4. Simultaneously, the CH_2O fraction increases and becomes more pronounced at temperatures above ~400°C, continuing to increase at 550°C. Overall, GO/SiO_2 shows low conversion, with DME formation occurring only in an intermediate-temperature range.

Figure 4b shows the temperature dependence of the product composition during methanol conversion over the rGO/SiO_2 catalyst. In the low-temperature region up to ~300°C, product formation is minimal

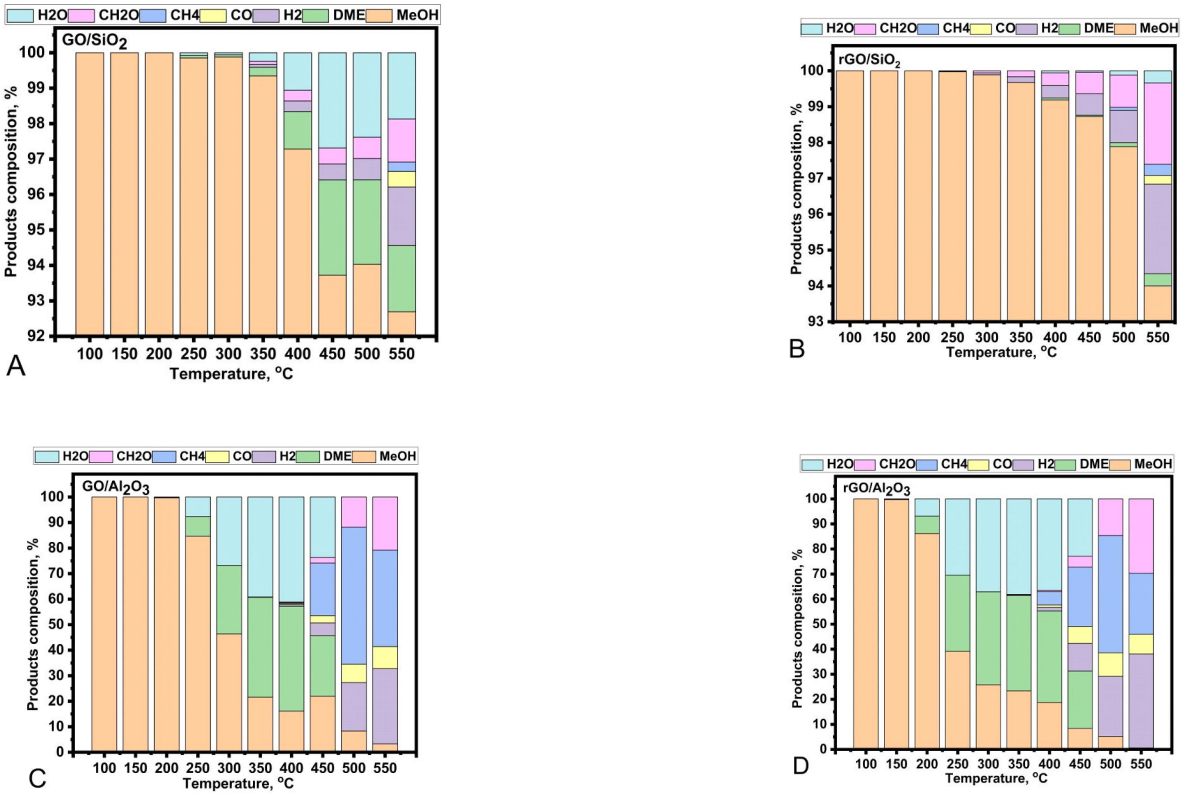

Fig. 4. Temperature dependence of composition of reaction products in the temperature range of 100–400°C. Methanol conversion on GO/SiO_2 (a); rGO/SiO_2 (b); GO/Al_2O_3 (c); and rGO/Al_2O_3 (d)

and the mixture is dominated by unreacted methanol, indicating negligible conversion. Starting from ~350–400°C, a gradual increase in the total amount of products is observed, suggesting activation of methanol conversion at elevated temperatures. In the high-temperature range ~400–550°C, the contribution of gaseous products increases, particularly H_2, together with the appearance and growth of CO. At the same time, CH_2O formation becomes noticeable and increases with temperature, reaching its highest fraction at 550°C. The contribution of CH_4 remains relatively low compared with other gas-phase products. DME is formed mainly at elevated temperatures and constitutes only a secondary product, indicating that the methanol dehydration pathway is not dominant over the rGO/SiO_2 catalyst. H_2O is formed predominantly in the higher temperature region and increases with temperature, although it does not represent the major component of the product mixture.

Figure 4c shows the temperature dependence of the product composition during methanol conversion over the GO/Al_2O_3 catalyst. Starting from 250°C, a sharp increase in the total amount of products is observed, and the dominant products become DME and H_2O, confirming that methanol dehydration is the main pathway in the intermediate temperature region. The DME contribution remains high up to 400°C, accompanied by significant H_2O formation as a coproduct. With further temperature increase, the DME fraction decreases markedly, whereas the contribution of gaseous products increases. At elevated temperatures above 450°C, CH_4 and H_2 become major components of the mixture, CO also increases, and a pronounced growth of CH_2O is observed, indicating enhancement of high-temperature methanol conversion routes.

Figure 4d presents the temperature dependence of the product composition during methanol conversion over the rGO/Al_2O_3 catalyst. In the low-temperature region, methanol remains the main component. However, starting from 200°C, the product composition changes significantly. In the intermediate temperature range, both DME and H_2O are formed; however, compared with GO/Al_2O_3, the contribution of DME is less pronounced, while H_2O remains a major component. At higher temperatures, a strong increase in gaseous products is observed. In particular, the fractions of CH_4 and H_2 increase substantially, accompanied by a higher contribution of CO. In addition, at temperatures of 500–550°C the CH_2O fraction increases markedly, becoming one of the major oxygenated products.

The obtained results show that methanol conversion over graphene-derived catalysts is governed by the nature of the oxide support and by the chemical state of the graphene phase. Al_2O_3-supported systems demonstrate higher activity than SiO_2-supported ones, which is consistent with the presence of Lewis acidic sites and surface hydroxyl groups on γ-Al_2O_3 that promote methanol activation and dehydration reactions [28–31]. In contrast, the low intrinsic acidity of SiO, limits methanol activation, resulting in low conversion over the entire investigated temperature range [28,29].

Methanol conversion in the intermediate temperature range for the GO/Al_2O_3 catalyst proceeds mainly via dehydration to dimethyl ether with simultaneous water formation, indicating the involvement of alumina acidic sites. With increasing temperature, the contribution of DME decreases, while the fractions of H_2, CO, CH_4, and CH_2O increase. Therefore, at high temperatures, methanol does not form DME on Al_2O_3-supported samples, despite the presence of an acidic oxide support. In this temperature range, methanol conversion is associated with high-temperature pathways such as dehydrogenation, decomposition, and secondary transformations of oxygenated intermediates [32–34]. The formation of CH_4 at elevated temperatures indicates deeper transformation of methanol-derived intermediates under these conditions.

The decreased selectivity for the DME formation at high temperatures on Al_2O_3-supported catalysts can be explained by the increasing role of diffusion limitations. Under these conditions, methanol conversion occurs mainly at the outer surface of catalyst granules. Since this surface is covered by the graphene-derived phase, methanol interacts predominantly with reduced graphene oxide via redox-type pathways, leading to the formation of gaseous products and formaldehyde instead of dehydration products. Therefore, it can be proposed that at high temperatures, the main route of MeOH transformation on rGO is a dehydrogenation, which is consistent with previously obtained results for MWCNT [35–36].

For SiO_2-supported catalysts, methanol conversion remains low due to the weak acidity of the support; however, the chemical state of the graphene phase influences product distribution. The GO/SiO_2 sample shows limited DME formation in a narrow temperature range, which can be attributed to the presence of oxygen-containing functional groups introducing additional acidic character. In contrast, rGO/SiO_2 mainly promotes the formation of small amounts of gaseous products and CH_2O at high temperatures, consistent with the limited contribution of dehydration reactions on these systems [37–39].

Therefore, methanol conversion over graphene-derived catalysts is determined by the combined

influence of oxide support acidity, diffusion limitations, and surface coverage by the graphene-derived phase. The differences observed between Al_2O_3- and SiO_2-supported graphene-derived catalysts reflect the extent to which the oxide support participates in methanol conversion. While γ-Al_2O_3 promotes surface-mediated dehydration at intermediate temperatures, SiO_2-supported systems exhibit limited activity and product distributions dominated by high-temperature conversion products. Al_2O_3 promotes dehydration at intermediate temperatures, whereas at high temperatures, diffusion limitations and coverage of the external surface by reduced graphene oxide suppress DME formation and shift methanol conversion toward redox-type pathways.

Conclusions

It is demonstrated that methanol conversion over graphene-derived catalysts strongly depends on the nature of the oxide support. The SiO_2-supported catalysts are low active with only a slight increase in conversion above ~400^{0}C. In contrast, Al_2O_3-supported catalysts show substantially higher activity. Methanol conversion for rGO/Al, O reaches ~95−100% in the 450−550^{0}C temperature range, representing the highest and most stable performance among the investigated samples. Differences in product distribution between GO- and rGO-containing are conditioned by the oxidation degree. The more oxidized GO/Al_2O_3 shows higher selectivity for dimethyl ether, while H_2, CO, CH_4, and CH_2O, become dominant for rGO/Al_2O_3. It can be concluded that methanol conversion over graphene-derived catalysts is governed by oxide support acidity, diffusion limitations, and surface coverage by the graphene-derived phase. Al_2O_3 promotes methanol dehydration at intermediate temperatures, whereas diffusion limitations and coverage of the external surface by reduced graphene oxide suppress dimethyl ether formation at high temperatures and shift methanol conversion toward redox-type pathways.

Acknowledgments

This work was carried out with financial support from a grant provided by the Simons Foundation (ID: SFI-PD-Ukraine-00014577 (2025)).

Raman spectroscopy, thermogravimetric analysis (TGA), and scanning electron microscopy with elemental mapping (SEM−EDX) were performed at Nicolaus Copernicus University. The authors would like to thank Prof. Wojciech Kujawski, PhD, DSc, for his support.

REFERENCES

1. *Chmielarz L.* Dehydration of methanol to dimethyl ether − current state of the art and future prospects // Catalysts. − 2024. − Vol.14. − Art. No. 308.

2. *Effect* of the property of alumina catalysts on methanol dehydration to dimethyl ether / Takeguchi T., Yanagisawa K.I., Inui T., Inoue M. // Appl. Catal. A: Gen. − 2000. − Vol.192. − P.201-209.

3. *Influence* of structure type of Al_2O_3 on dehydration of methanol to dimethyl ether / Seo C.W., Jung K.D., Kim S.H., Song I.K. // Ind. Eng. Chem. Res. − 2008. − Vol.47. − No. 21. − P.8170-8175.

4. *Sahebdelfar S.* Deactivation kinetics of g-Al_2O_3 catalyst in methanol dehydration to dimethyl ether // Fuel. − 2022. − Vol.324. − Art. No. 124625.

5. *Carbocatalysis* by graphene-based materials / Navalon S., Dhakshinamoorthy A., Alvaro M., Garcia H. // Chem. Rev. − 2014. − Vol.114. − P.6179-6212.

6. *Methanol* to formaldehyde: an overview of surface studies and performance of an iron molybdate catalyst / Malik M.I., Abatzoglou N., Achouri I.E. // Catalysts. − 2021. − Vol.11. − No. 8. − Art. No. 893.

7. *Practical* carbocatalysis by graphene oxide nanosheets in aqueous medium / Kausar N., Dhavale V.M., Jadhav M. // RSC Adv. − 2016. − Vol.6. − P.73034-73042.

8. *Recent* advances in graphene oxide catalyzed organic transformations / Zhou Y., Kong X., Wang T., Xu F., Wang L. // Chin. Chem. Lett. − 2022. − Vol.33. − No. 3. − P.1501-1514.

9. *Graphene* oxide: an effective acid catalyst for the synthesis of polyoxymethylene dimethyl ethers from methanol and trioxymethylene / Wang R., Wu Z., Qin Z., Chen C., Dong M., Li S., et al. // Catal. Sci. Technol. − 2016. − Vol.6. − P.4488-4496.

10. *Reduced* graphene oxide as an excellent platform to obtain highly efficient recyclable solid acid catalysts / dos Santos T.C., La Porta F.A., Ferrer M.M., Lima R.C., Andres J., Longo E. // Fuel. − 2019. − Vol.248. − P.306-315.

11. *Nosach V.V., Bychko I.B., Strizhak P.E.* Catalytic properties of reduced graphene oxide deposited on aluminium oxide in the process of ethane dehydrogenation // Theor. Exp. Chem. − 2025. − Vol.61. − P.141-147.

12. *Socrates G.* Infrared and Raman characteristic group frequencies: tables and charts (3rd ed.). − Wiley. 2001.

13. *Busca G.* The surface of transitional aluminas: a critical review // Catal. Today. − 2014. − Vol.226. − P.2-13.

14. *The chemistry* of graphene oxide / Dreyer D.R., Park S., Bielawski C.W., Ruoff R.S. // Chem. Soc. Rev. − 2010. − Vol.39. − P.228-240.

15. *Pei S., Cheng H.M.* The reduction of graphene oxide // Carbon. − 2012. − Vol.50. − P.3210-3228.

16. *Galeener F.L.* Planar rings in vitreous silica // Phys. Rev. B. − 1979. − Vol.19. − P.4292-4297.

17. *Busca G.* Acidity and basicity of aluminas: characterization and catalytic activity // Catal. Today. – 2020. – Vol.357. – P.621-629.

18. *Ferrari A.C.* Raman spectroscopy of graphene and graphite // Solid State Commun. – 2007. – Vol.143. – P.47-57.

19. *Quantifying* defects in graphene via Raman spectroscopy at different excitation energies / Cancado L.G., Jorio A., Ferreira E.H.M., Stavale F., Achete C.A., Capaz R.B., et al. // Nano Lett. – 2011. – Vol.11. – P.3190-3196.

20. *Probing* the nature of defects in graphene by Raman spectroscopy / Eckmann A., Felten A., Mishchenko A., Britnell L., Krupke R., Novoselov K.S., et al. // Nano Lett. – 2012. – Vol.12. – P.3925-3930.

21. *Ferrari A.C., Basko D.M.* Raman spectroscopy as a versatile tool for studying graphene // Nat. Nanotechnol. – 2013. – Vol.8. – P.235-246.

22. *Synthesis*, dispersion, and cytocompatibility of graphene oxide / Aleksandrzak M., Chen X., Kalenczuk R.J., Borowiak-Palen E. // Colloids Surf. B. – 2011. – Vol.89. – P.79-85.

23. *Detailed* thermal reduction analyses of graphene oxide via in-situ TEM/EELS studies / Pelaez-Fernandez M., Bermejo A., Benito A.M., Maser W.K., Arenal R. // Carbon. – 2021. – Vol.178. – P.477-487.

24. *Critical* temperatures in the synthesis of graphene-like materials by thermal exfoliation–reduction of graphite oxide / Botas C., Alvarez P., Blanco C., Santamaria R., Granda M., Ares P., et al. // Carbon. – 2013. – Vol.52. – P.476-485.

25. *Thermogravimetric* analysis of graphene materials / Farivar F., Yap P.L., Hassan K., Tung T.T., Tran D.N.H., Losic D. // C. – 2021. – Vol.7. – No. 2. – Art. No. 41.

26. *Kinetics* of the thermal decomposition of thermally reduced graphene oxide in hydrogen atmosphere / Dolbin O.V., Vinnikov N.A., Gavrilko V.G., Chuyev V.P., Eselson V.B., Khrapak A.G. // Low Temp. Phys. – 2024. – Vol.50. – No. 3. – P.305-311.

27. *Enhancing* dimethyl ether production as a renewable fuel in a catalytic membrane reactor with BEA zeolite / Avruscio E., Sabir A.W., Barbieri G., Lee P.S., Catizzone E., Migliori M., et al. // Renewable Energy. – 2025. – Vol.238. – Art. No. 124187.

28. *Methanol* dehydration to dimethyl ether on ball milling-derived high-surface-area alpha-alumina catalysts / Agbaba O., Amrute A.P., Ochoa-Hernandez C., Triller S., Schuth F. // ChemCatChem. – 2024. – Vol.16. – No. 4. – Art. No. e202301159.

29. *Bercic G., Levec J.* Modeling of an industrial fixed-bed reactor to produce dimethyl ether from methanol // Chem. Eng. Sci. – 1993. – Vol.48. – No. 2. – P.397-409.

30. *Methanol* dehydration to dimethyl ether over Al_2O_3 catalysts / Akarmazyan S.S., Panagiotopoulou P., Kambolis A., Kondarides D.I. // Appl. Catal. B: Environ. – 2013. – Vol.134-135. – P.286-294.

31. *Olah G.A., Goeppert A., Prakash G.K.S.* Chemical recycling of carbon dioxide to methanol and dimethyl ether // J. Org. Chem. – 2009. – Vol.74. – No. 2. – P.487-498.

32. *Usman M., Yamada T.* Methanol reforming for hydrogen production // ACS Eng. Au. – 2025. – Vol.5. – No. 4. – P.314-346.

33. *Reaction* pathways of methanol formation in CO_2 hydrogenation / Makhmutov D., Fedorova E.A., Zanina A., Kubis C., Zhao D., Doronkin D.E., et al. // ACS Catal. – 2025. – Vol.15. – No. 3. – P.2328-2341.

34. *Eigler S., Hirsch A.* Chemistry with graphene and graphene oxide – challenges for synthetic chemists // Angew. Chem. Int. Ed. – 2014. – Vol.53. – P.7720-7738.

35. *Acid–base* and redox performance of carbon nanotubes in methanol conversion / Bychko I., Abakumov A., Zhokh A., Trypolskyi A., Kremen O., Strizhak P. // Catal. Sci. Technol. – 2025. – Vol.15. – P.1581-1593.

36. *Dependence* of structure of multilayer graphene oxide on degree of graphitization of initial graphite / Abakumov A.A., Bychko I.B., Nikolenko A.S., Strizhak P.E. // Theor. Exp. Chem. – 2018. – Vol.54. – P.186-192.

37. *Alka Patel U.K., Agarwal A.* Carbocatalytic activity of graphene oxide in organic transformations: a comprehensive review // ChemistrySelect. – 2025. – Vol.10. – No. 22. – Art. No. e01118.

38. *Catalytic* dehydration of methanol to dimethyl ether (DME) over Al-HMS catalysts / Sabour B., Peyrovi M.H., Hamoule T., Rashidzadeh M. // J. Ind. Eng. Chem. – 2013. – Vol.19. – No. 5. – P.1578-1583.

39. *Direct* dehydrogenation of methanol to formaldehyde over ZnO–SiO_2-based catalysts / Chowdhury A.G., Arnold U., Garbev K., Bender M., Sauer J. // Catal. Sci. Technol. – 2024. – Vol.14. – P.4958-4967.

Received 14.10.2025
Revised 18.12.2025
Accepted 23.01.2026
Published 25.02.2026

КАТАЛІТИЧНІ ВЛАСТИВОСТІ ОКСИДУ ГРАФЕНУ ТА ВІДНОВЛЕНОГО ОКСИДУ ГРАФЕНУ, НАНЕСЕНИХ НА АЛЮМІНІЙ ТА КРЕМНІЙ ОКСИДИ, У ПРОЦЕСІ ПЕРЕТВОРЕННЯ МЕТАНОЛУ

В.В. Носач, І.Б. Бичко, П.Є. Стрижак

Каталітичні властивості оксиду графену та відновленого оксиду графену, нанесених на Al_2O_3 і SiO_2, досліджено в реакції перетворення метанолу. Встановлено суттєвий вплив оксидного носія та хімічного стану графеновмісної фази на каталітичну активність і склад продуктів реакції. Каталізатори, нанесені на SiO_2, характеризуються низькою активністю, тоді як системи на основі Al_2O_3 забезпечують значно вищу конверсію метанолу. Для матеріалів Al_2O_3 у середньотемпературному діапазоні спостерігається утворення диметилового етеру, тоді як за вищих температур перетворення метанолу зміщується в бік утворення високотемпературних продуктів, зокрема H_2, CO, CH_4 і CH_2O. Таке зміщення може бути пов'язане з дифузійними обмеженнями та покриттям поверхні фазою відновленого оксиду графену. Отримані результати свідчать, що шляхи перетворення метанолу на графеновмісних каталізаторах можуть бути цілеспрямовано регульовані через поєднання властивостей оксидного носія та контрольованого ступеня відновлення оксиду графену.

Ключові слова*:* оксид графену, відновлений оксид графену, алюміній оксид, кремній оксид, перетворення метанолу, карбокаталіз.

CATALYTIC PROPERTIES OF GRAPHENE OXIDE AND REDUCED GRAPHENE OXIDE SUPPORTED ON ALUMINA AND SILICA IN METHANOL CONVERSION

V.V. Nosach [a, b, *], I.B. Bychko [a], P.Ye. Strizhak [a]

[a] L.V. Pisarzhevskii Institute of Physical Chemistry of National Academy of Sciences of Ukraine, Kyiv, Ukraine

[b] National University of «Kyiv-Mohyla Academy», Kyiv, Ukraine

[*] e-mail: victorynosach@gmail.com

The catalytic properties of graphene oxide and reduced graphene oxide supported on Al_2O_3 and SiO_2 were studied in methanol conversion. The results show the strong influence of the support and the chemical state of the graphene-derived phase on catalytic activity and product formation. SiO_2-supported catalysts provide low activity, whereas Al_2O_3-supported systems demonstrate significantly higher methanol conversion. Methanol conversion on Al_2O_3-supported materials leads to dimethyl ether formation in the intermediate temperature range, while at higher temperatures, methanol conversion shifts toward high-temperature products, including H_2, CO, CH_4, and CH_2O. This shift can be associated with diffusion limitations and surface coverage by the reduced graphene oxide phase. The study shows that methanol conversion pathways over graphene-derived catalysts can be tuned by combining oxide support properties with controlled reduction of graphene oxide.

Keywords*:* graphene oxide; reduced graphene oxide; alumina; silica; methanol conversion; carbocatalysis.

REFERENCES

1. Chmielarz L. Dehydration of methanol to dimethyl ether – current state of the art and future prospects. *Catalysts.* 2024; 14: 308. doi: 10.3390/catal14050308.

2. Takeguchi T, Yanagisawa KI, Inui T, Inoue M. Effect of the property of alumina catalysts on methanol dehydration to dimethyl ether. *Appl Catal A Gen.* 2000; 192: 201-209. doi: 10.1016/S0926-860X(99)00374-8.

3. Seo CW, Jung KD, Kim SH, Song IK. Influence of structure type of Al_2O_3 on dehydration of methanol to dimethyl ether. *Ind Eng Chem Res.* 2008; 47(21): 8170-8175. doi: 10.1021/ie800106e.

4. Sahebdelfar S. Deactivation kinetics of g-Al_2O_3 catalyst in methanol dehydration to dimethyl ether. *Fuel.* 2022; 324: 124625. doi: 10.1016/j.fuel.2022.124625.

5. Navalon S, Dhakshinamoorthy A, Alvaro M, Garcia H. Carbocatalysis by graphene-based materials. *Chem Rev.* 2014; 114: 6179-6212. doi: 10.1021/cr4007347.

6. Malik MI, Abatzoglou N, Achouri IE. Methanol to formaldehyde: an overview of surface studies and performance of an iron molybdate catalyst. *Catalysts.* 2021; 11(8): 893. doi: 10.3390/catal11080893.

7. Kausar N, Dhavale VM, Jadhav M. Practical carbocatalysis by graphene oxide nanosheets in aqueous medium. *RSC Adv.* 2016; 6: 73034-73042. doi: 10.1039/C6RA17520A.

8. Zhou Y, Kong X, Wang T, Xu F, Wang L. Recent advances in graphene oxide catalyzed organic transformations. *Chin Chem Lett.* 2022; 33(3): 1501-1514. doi: 10.1016/j.cclet.2021.10.081.

9. Wang R, Wu Z, Qin Z, Chen C, Dong M, Li S, et al. Graphene oxide: an effective acid catalyst for the synthesis of polyoxymethylene dimethyl ethers from methanol and trioxymethylene. *Catal Sci Technol.* 2016; 6: 4488-4496. doi: 10.1039/C5CY01854D.

10. dos Santos TC, La Porta FA, Ferrer MM, Lima RC, Andres J, Longo E. Reduced graphene oxide as an excellent platform to obtain highly efficient recyclable solid acid catalysts. *Fuel.* 2019; 248: 306-315. doi: 10.1016/j.fuel.2019.115793.

11. Nosach VV, Bychko IB, Strizhak PE. Catalytic properties of reduced graphene oxide deposited on aluminium oxide in the process of ethane dehydrogenation. *Theor Exp Chem.* 2025; 61: 141-147. doi: 10.1007/s11237-025-09860-w.

12. Socrates G. *Infrared and Raman characteristic group frequencies: tables and charts* (3rd ed.). Wiley; 2001.

13. Busca G. The surface of transitional aluminas: a critical review. *Catal Today.* 2014; 226: 2-13. doi: 10.1016/j.cattod.2013.08.039.

14. Dreyer DR, Park S, Bielawski CW, Ruoff RS. The chemistry of graphene oxide. *Chem Soc Rev.* 2010; 39: 228-240. doi: 10.1039/B917103G.

15. Pei S, Cheng HM. The reduction of graphene oxide. *Carbon.* 2012; 50: 3210-3228. doi: 10.1016/j.carbon.2011.11.010.

16. Galeener FL. Planar rings in vitreous silica. *Phys Rev B.* 1979; 19: 4292-4297. doi: 10.1103/PhysRevB.19.4292.

17. Busca G. Acidity and basicity of aluminas: characterization and catalytic activity. *Catal Today*. 2020; 357: 621-629. doi: 10.1016/j.cattod.2019.03.014.

18. Ferrari AC. Raman spectroscopy of graphene and graphite. *Solid State Commun*. 2007; 143: 47-57. doi: 10.1016/j.ssc.2007.03.052.

19. Cancado LG, Jorio A, Ferreira EHM, Stavale F, Achete CA, Capaz RB, et al. Quantifying defects in graphene via Raman spectroscopy at different excitation energies. *Nano Lett.* 2011; 11: 3190-3196. doi: 10.1021/nl201432g.

20. Eckmann A, Felten A, Mishchenko A, Britnell L, Krupke R, Novoselov KS, et al. Probing the nature of defects in graphene by Raman spectroscopy. *Nano Lett.* 2012; 12: 3925-3930. doi: 10.1021/nl300901a.

21. Ferrari AC, Basko DM. Raman spectroscopy as a versatile tool for studying graphene. *Nat Nanotechnol.* 2013; 8: 235-246. doi: 10.1038/nnano.2013.46.

22. Aleksandrzak M, Chen X, Kalenczuk RJ, Borowiak-Palen E. Synthesis, dispersion, and cytocompatibility of graphene oxide. *Colloids Surf B*. 2011; 89: 79-85. doi: 10.1016/j.colsurfb.2011.08.026.

23. Pelaez-Fernandez M, Bermejo A, Benito AM, Maser WK, Arenal R. Detailed thermal reduction analyses of graphene oxide via in-situ TEM/EELS studies. *Carbon.* 2021; 178: 477-487. doi: 10.1016/j.carbon.2021.03.018.

24. Botas C, Alvarez P, Blanco C, Santamaria R, Granda M, Ares P, et al. Critical temperatures in the synthesis of graphene-like materials by thermal exfoliation–reduction of graphite oxide. *Carbon*. 2013; 52: 476-485. doi: 10.1016/j.carbon.2012.09.059.

25. Farivar F, Yap PL, Hassan K, Tung TT, Tran DNH, Losic D. Thermogravimetric analysis of graphene materials. *C.* 2021; 7(2): 41. doi: 10.3390/c7020041.

26. Dolbin OV, Vinnikov NA, Gavrilko VG, Chuyev VP, Eselson VB, Khrapak AG. Kinetics of the thermal decomposition of thermally reduced graphene oxide in hydrogen atmosphere. *Low Temp Phys.* 2024; 50(3): 305-311. doi: 10.1063/10.0025619.

27. Avruscio E, Sabir AW, Barbieri G, Lee PS, Catizzone E, Migliori M, et al. Enhancing dimethyl ether production as a renewable fuel in a catalytic membrane reactor with BEA zeolite. *Renewable Energy*. 2025; 238: 124187. doi: 10.1016/j.renene.2025.124187.

28. Agbaba O, Amrute AP, Ochoa-Hernandez C, Triller S, Schuth F. Methanol dehydration to dimethyl ether on ball milling-derived high-surface-area alpha-alumina catalysts. *ChemCatChem*. 2024; 16(4): e202301159. doi: 10.1002/cctc.202301159.

29. Bercic G, Levec J. Modeling of an industrial fixed-bed reactor to produce dimethyl ether from methanol. *Chem Eng Sci.* 1993; 48(2): 397-409.

30. Akarmazyan SS, Panagiotopoulou P, Kambolis A, Kondarides DI. Methanol dehydration to dimethyl ether over Al_2O_3 catalysts. Appl Catal B Environ. 2013; 134-135: 286-294. doi: 10.1016/j.apcatb.2012.11.043.

31. Olah GA, Goeppert A, Prakash GKS. Chemical recycling of carbon dioxide to methanol and dimethyl ether. *J Org Chem*. 2009; 74(2): 487-498. doi: 10.1021/jo801260f.

32. Usman M, Yamada T. Methanol reforming for hydrogen production. *ACS Eng Au*. 2025; 5(4): 314-346. doi: 10.1021/acsengineeringau.5c00031.

33. Makhmutov D, Fedorova EA, Zanina A, Kubis C, Zhao D, Doronkin DE, et al. Reaction pathways of methanol formation in CO_2 hydrogenation. *ACS Catal.* 2025; 15(3): 2328-2341. doi: 10.1021/acscatal.4c07462.

34. Eigler S, Hirsch A. Chemistry with graphene and graphene oxide – challenges for synthetic chemists. *Angew Chem Int Ed.* 2014; 53: 7720-7738. doi: 10.1002/anie.201402780.

35. Bychko I, Abakumov A, Zhokh A, Trypolskyi A, Kremen O, Strizhak P. Acid–base and redox performance of carbon nanotubes in methanol conversion. *Catal Sci Technol.* 2025; 15: 1581-1593. doi: 10.1039/D4CY01109K.

36. Abakumov AA, Bychko IB, Nikolenko AS, Strizhak PE. Dependence of structure of multilayer graphene oxide on degree of graphitization of initial graphite. *Theor Exp Chem*. 2018; 54: 186-192. doi: 10.1007/s11237-018-9560-z.

37. Alka Patel UK, Agarwal A. Carbocatalytic activity of graphene oxide in organic transformations: a comprehensive review. *ChemistrySelect.* 2025; 10(22): e01118. doi: 10.1002/slct.202501118.

38. Sabour B, Peyrovi MH, Hamoule T, Rashidzadeh M. Catalytic dehydration of methanol to dimethyl ether (DME) over Al-HMS catalysts. *J Ind Eng Chem.* 2013; 19(5): 1578-1583. doi: 10.1016/j.jiec.2013.03.044.

39. Chowdhury AG, Arnold U, Garbev K, Bender M, Sauer J. Direct dehydrogenation of methanol to formaldehyde over ZnO–SiO_2-based catalysts. Catal Sci Technol. 2024; 14: 4958-4967. doi: 10.1039/D4CY00541D.